J. Fluid Mech. (2008), *vol.* 615, *pp.* 169–184.
doi:10.1017/S0022112008003546 Printed in the United Kingdom

Two-layer hydraulics for a co-located crest and narrows

LAURENCE ARMI[1] AND ULRIKE RIEMENSCHNEIDER[2]

[1]Scripps Institution of Oceanography, La Jolla, CA 92093-0225, USA
[2]St Columba's College, Whitechurch, Dublin 16, Ireland

(Received 18 October 2007 and in revised form 15 July 2008)

The theory of two-layer hydraulics is extended to topography with co-varying width and height. When these variations of the non-dimensional width and total depth have a power law relationship, the solutions can still be presented in the Froude-number plane for both unidirectional and exchange flows. These differ from previous solutions, which were limited to treating width and height variations separately.

1. Introduction

The internal hydraulics of two-layer flows has application to many geophysical and practical problems. In Armi (1986), these flows are parameterized in terms of the internal Froude numbers for each layer. The possible steady-flow solutions are then shown in the Froude-number plane. Conditions for critical flow take a particularly simple form as a straight line in the Froude-number plane and this presentation allows all solutions to be seen at once.

Among an infinite number of non-unique possible steady flows, hydraulics can be used to search out those that are asymmetric. The existence of a unique steady asymmetric solution is an empirical fact, for example, we talk about flows over a sill or through a strait. The flow must be asymmetric in the sense that it must connect two reservoirs with different fluid depths. For a single layer, only one such possible flow exists and this asymmetric flow is called controlled because certain distinct regularity conditions must be satisfied for its existence. For two layers of comparable depths and flow rates, two unique controlled asymmetric flows are often possible. One controlled asymmetric solution has the lower layer as the active layer and looks like the familiar single-layer flow. The other unique solution has the upper layer as the active layer. Which of the two asymmetric flows is realized depends on which asymmetric solution is required to match the different reservoir conditions. For two-layer flows, there is the additional concept of a virtual control, first introduced by Wood (1968). Control need not occur at a topographically obvious location, such as the narrowest section. As the flow rates for a two-layer flow increase, there may no longer be the possibility of the two asymmetric solutions satisfying critical conditions at the topographic control. They, in fact, merge upstream and the control moves upstream as a virtual control, satisfying critical conditions at a deeper/wider section upstream. For a two-layer unidirectional flow through a simple contraction, the virtual control imposes no shear. For exchange flows through a contraction, the virtual control imposes equal and opposite velocities. For the co-located crest and narrows studied here, the result will be seen to be more complicated.

A past limitation of the Froude-number plane and the extension of the theory to maximal exchange flows by Armi & Farmer (1986) and Farmer & Armi (1986) was that separate planes were required for contractions and sills. This is because there is a fundamental difference between flow through a contraction and flow over a sill. A sill only directly contacts the bottom layer, and the upper layer's response is indirect. In contrast, a contraction directly contacts both layers. Dalziel (1991) offers an alternative formulation of the two-layer hydraulic problem by extending the functional formalism applied by Gill (1977) to single-layer problems. This formalism is applied to maximal exchange in channels with non-rectangular cross-sections in Dalziel (1992), but attention is confined to a relatively simple class of along-channel geometries where width and depth variations are isolated. Farmer & Armi also isolated the sill from the exit expansion control. The extension to continuous stratification has also been limited to separate consideration of sills and contractions. The solution for unidirectional stratified flow through a non-rectangular channel, presented by Engqvist & Hogg (2004), is restricted to geometries where the bottom is flat.

Riemenschneider, Smeed & Killworth (2005) showed that for a particular rectangular channel where the width is proportional to the square root of the depth, a pseudo-Froude-number plane can be used to represent all possible solutions for a rotating exchange flow. Inspired by this fact, the theory of Armi (1986) for non-rotating two-layer hydraulics is extended here to a topography with co-varying width and depth. This extension makes the application to geophysical problems more realistic since, in many of these applications, the highest point or crest and the narrowest width coincide.

2. Hydraulic theory and the Froude-number plane

The two-layer theory for hydraulic flows (Armi 1986) is based on the assumptions that the flow is frictionless, uniform, one-dimensional and hydrostatic. Here, we review this theory and apply the generalization to co-varying topography. The Bernoulli (energy) equations and the equations of continuity are cast in dimensionless form using the Froude numbers, $F_1 = u_1/\sqrt{g'y_1}$ and $F_2 = u_2/\sqrt{g'y_2}$, of the top and bottom layer, respectively. They combine to form the composite Froude number, which is equal to unity when the flow is critical,

$$G^2 = F_1^2 + F_2^2 = 1. \tag{2.1}$$

The critical condition (2.1) collapses to a straight line in the Froude-number plane. This straight line will clearly show the controls, both topographic and virtual, which must lie on the line, and separates subcritical ($G^2 < 1$) from supercritical flow ($G^2 > 1$).

The flows considered are steady, and the flow rate along the channel is specified by $q_i = u_i b y_i$ for each layer. This is the continuity equation describing the conserved transport in each of the two layers along the channel. All the topographic variables are shown in figure 1. The velocity in each layer is u_i; b_0 and b_v are widths associated with the narrowest topographic section and virtual control, when one exists. Using the definition of the Froude numbers and the continuity equation, u_i and y_i can be rewritten in terms of the Froude number and the layer transport:

$$y_i = \left[\frac{q_i^2}{b^2 g'}\right]^{1/3} F_i^{-2/3}, \tag{2.2}$$

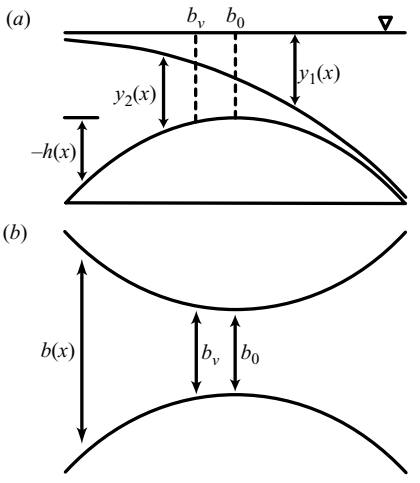

FIGURE 1. Sketch of the channel topography and notation. (*a*) Side view of the channel with layers 1 and 2, top and bottom layer, respectively. The controls are marked by vertical dashed lines and labelled b_0 for the primary control at the top of the sill, and b_v at the virtual control. (*b*) Plan view of the channel.

and similarly,

$$u_i = \left[\frac{q_i g'}{b}\right]^{1/3} F_i^{2/3}. \tag{2.3}$$

The non-dimensional parameters of the problem are given by:

$$\left.\begin{aligned} b' &= b/b_0, \\ h' &= h/(y_1 + y_2)_0, \\ y_i' &= y_i/(y_1 + y_2)_0, \end{aligned}\right\} \tag{2.4}$$

where $(y_1 + y_2)_0$ is defined to be the depth at the sill crest, which for the treatment here must coincide with the narrows. Note, with this definition, h' will always be negative and the non-dimensional total depth is $(1 - h')$. Hence, the non-dimensional volume flow rate is defined by:

$$q_i' = \frac{q_i}{g'^{1/2} b_0 (y_1 + y_2)_0^{3/2}}. \tag{2.5}$$

The non-dimensional form of the continuity equation (2.2) for each layer becomes

$$y_i' = \left[\frac{q_i'}{b'}\right]^{2/3} F_i^{-2/3}. \tag{2.6}$$

Combining this with the equation describing the level free surface (rigid-lid approximation):

$$y_1' + y_2' + h' = 1, \tag{2.7}$$

we obtain:

$$\left[\frac{q_2'}{b'(1 - h')^{3/2}}\right]^{-2/3} = q_r^{2/3} F_1^{-2/3} + F_2^{-2/3}, \tag{2.8}$$

where $q_r = q_1/q_2$, the ratio of flow rates.

This equation defines loci in the Froude-number plane of possible combinations of internal Froude numbers for discrete values of the non-dimensional volume flow rate per unit width.

The Bernoulli equations for the two layers are:

$$H_1 = \tfrac{1}{2}\rho_1 u_1^2 + \rho_1 g(y_1 + y_2 + h) + p, \tag{2.9}$$

$$H_2 = \tfrac{1}{2}\rho_2 u_2^2 + \rho_1 g y_1 + \rho_2 g(y_2 + h) + p. \tag{2.10}$$

With a small density difference and a level free surface, subtracting (2.10) from (2.9) and combining with (2.6), we obtain:

$$Y_1' \left[\frac{q_2'}{b'}\right]^{-2/3} = q_r^{2/3}\left[F_1^{-2/3} + \tfrac{1}{2}F_1^{4/3}\right] - \tfrac{1}{2}F_2^{4/3}, \tag{2.11}$$

where Y_1' is defined as:

$$Y_1' = \frac{H_1 - H_2}{g'\rho_2(y_1 + y_2)_0} + 1. \tag{2.12}$$

To show all possible solutions in a single Froude-number plane, Armi (1986) split the cases into either pure contraction or pure sill flows. For contractions, the continuity equation (2.8) then contains only width dependence, and after substitution of this simpler equation into the Bernoulli equation (2.11), the flow rate per unit width disappears from the Bernoulli equation. For any flow ratio, q_r, this allows convenient plotting of curves with constant values of the Bernoulli constant in the Froude-number plane against the background formed by the loci of the continuity equation (2.8). The non-dimensional Bernoulli constant for the contraction is simply the interface height above the bottom in a stagnant reservoir. In the absence of dissipation, the Bernoulli constant is conserved, and hence any solution could be easily followed as the width varied. In particular, the asymmetric flows controlled by the critical condition (2.1) could easily be found. Also, the importance of virtual controls first found by Wood (1968) could easily be seen for unidirectional flows. The role of two controls for exchange flows, one at the narrowest section and one virtual, was discussed using this same framework by Armi & Farmer (1986).

For sills in a constant-width channel, the width dependence disappears in both the continuity (2.8) and Bernoulli (2.11) equations. Curves with constant values of the Bernoulli constant were again plotted in the Froude-number plane and any solution could easily be followed as the depth varied. Although virtual controls were found for the contraction case, for sill flows, only topographic controls at the sill crest or approach controls (Lawrence 1993) are seen.

For the cases we are considering here, we assume that the topography varies in such a way that the non-dimensional total depth and the non-dimensional width of the channel are everywhere connected by the following relationship:

$$(1 - h')^{3/2} = b'^{\alpha}. \tag{2.13}$$

Since (2.13) is non-dimensional, the aspect ratio of width to total depth at the narrowest section/crest can be quite arbitrary and the variation of the aspect ratio along the channel can include a variety of channels as long as the variation is given by a power law. If we substitute this expression into (2.8) we find:

$$\frac{q_2'}{b'^{(\alpha+1)}} = \left[q_r^{2/3}F_1^{-2/3} + F_2^{-2/3}\right]^{-3/2}. \tag{2.14}$$

This equation is the continuity equation for a fixed flow ratio, q_r. Contours of $q_2'/b'^{(\alpha+1)}$ are labelled in the background of each Froude-number plane (cf. figure 2*a*). These contours are the same as those in the background used by Armi (1986) (our equation (2.8)). However, the values of the contours shown throughout this paper combine the variations of width and height, whereas previously contractions and sills were treated independently.

Substituting (2.14) into (2.11) gives the new Bernoulli function:

$$Y_1'(q_2')^{-2\alpha/3(\alpha+1)} = \frac{q_r^{2/3}\left[F_1^{-2/3} + \frac{1}{2}F_1^{4/3}\right] - \frac{1}{2}F_2^{4/3}}{\left[q_r^{2/3}F_1^{-2/3} + F_2^{-2/3}\right]^{1/(\alpha+1)}}. \tag{2.15}$$

For what follows, we take $\alpha = 1$; however, cases with other values of α in (2.13) can be treated in the same manner. The Bernoulli function (2.15) is plotted for discreet values of $Y_1'(q_2')^{-1/3}$ against the background loci given by (2.14) in the Froude-number planes shown in figure 2 for values of $q_r = 1.0$, 0.5 and 2.0. The solutions of the energy equation are shown as heavy lines overlying the loci of constant non-dimensional flow rates. Unlike the solutions for flow through a pure contraction found in Armi (1986, figure 3*a*, *b*) the solutions are not symmetric with respect to each of the two layers. Whereas for a pure contraction, solutions for which the volume–flow ratio has a reciprocal value ($q_r = 2.0$) to that shown in figure 2(*b*) ($q_r = 0.5$) could be found by merely interchanging the roles of the two layers, here separate solution curves are required (figure 2*c*).

In the following sections, we discuss three types of flow solutions: flows with a single control at the crest/narrows; exchange flows; and unidirectional virtually controlled flows. For all the sketches of the flows, we have taken the topographic variation to be given by

$$(1 - h') = 1 + (x/2)^2. \tag{2.16}$$

For the cases that follow, we take for simplicity only, $q_r = 1$, hence we will be discussing solutions in the Froude-number plane represented by figure 2(*a*). At the crest/narrows, $b' = 1$, the term on the left-hand side of the continuity equation (2.14) is then simply the non-dimensional flow rate q_2'. This sets the value of the left-hand side of the continuity equation (2.15) at $b' = 1$. Depending on where in the Froude-number plane this curve lies we have the cases now described in the subsequent sections.

3. Flows with a single control at the crest/narrows

With moderate flow rates, two possible controlled flows are possible. (i) The upper layer dominates the dynamics and is accelerated; the interface rises downstream of the crest/narrows. (ii) The lower layer dominates and is accelerated as the interface descends downstream of the crest/narrows. As seen in Armi (1986), only the lower layer can dominate for a pure sill flow, yet both types are possible for a pure contraction. As an example, inspection of figure 2(*a*) shows that $q_2' = 0.2$ intersects the critical flow line, $F_1^2 + F_2^2 = 1$, at two locations in the Froude-number plane. Each of these intersections is associated with a controlled flow described below in which either the lower or upper layer dominates. The limiting value of the non-dimensional flow rate $q_2' < 0.226$ is seen in figure 2(*a*) for $q_r = 1$. For $q_r = 0.5$ shown in the Froude-number plane in figure 2(*b*), the limiting values is $q_2' < 0.5$.

A flow for which the lower layer dominates is shown on the left-hand side in figure 3 together with its associated solution curve, $Y_1'(q_2')^{-1/3} = 0.9$, in the

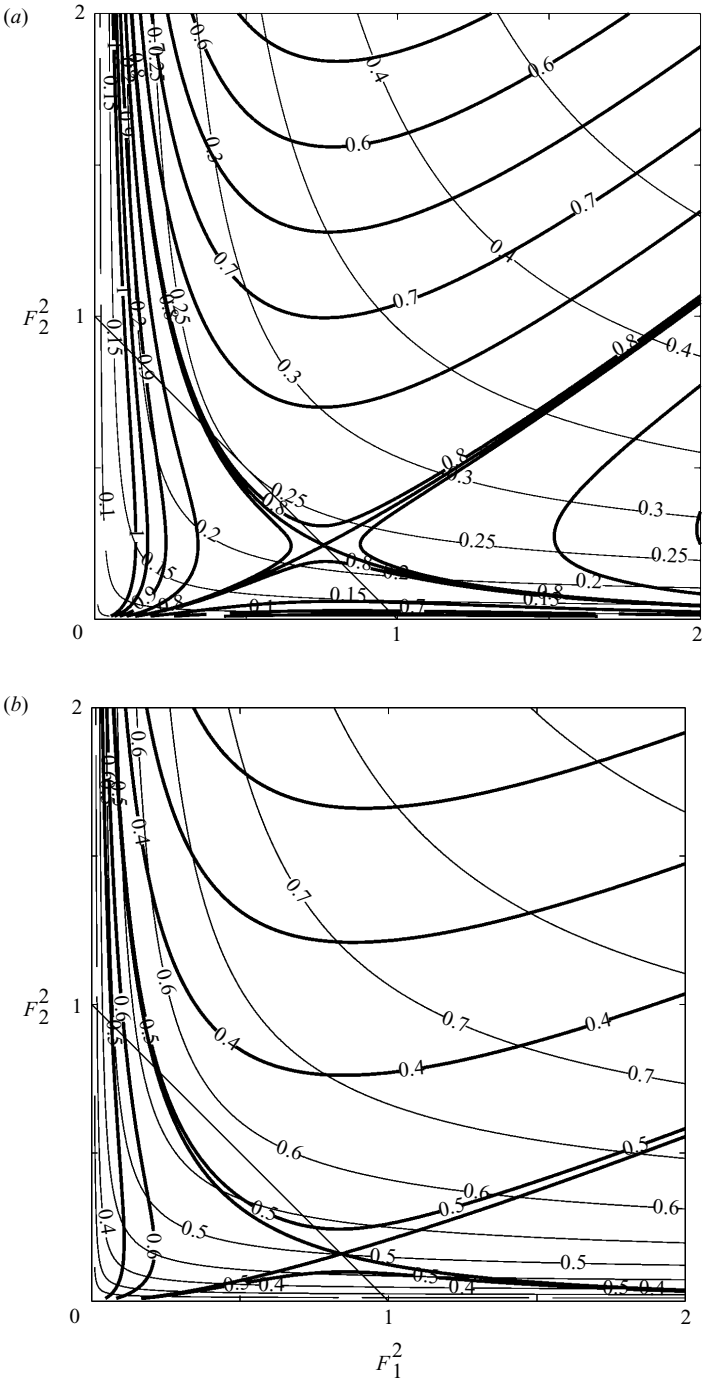

FIGURE 2(*a*, *b*). For caption see facing page.

Froude-number plane. The interface position is to scale from the actual solution found using the Froude-number-plane framework. Values of the solution parameters at the crest, upstream and downstream, can be found in table 1. To distinguish the fact that layer 2, the lower layer, is dominant in the dynamics, the crest/narrows is

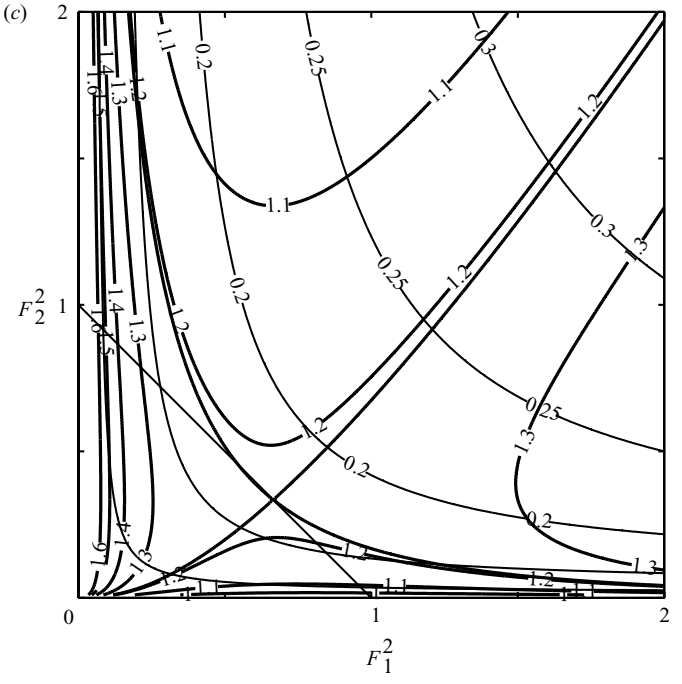

FIGURE 2. Froude-number plane for co-varying topography. (*a*) $q_r = 1$, (*b*) $q_r = 0.5$, (*c*) $q_r = 2$.

labelled b_{0_2}. The downstream value given in the table is from where the solution curve exits the Froude-number plane as drawn here ($F_2^2 = 2.0$). In the deep reservoir up stream, the interface depth is $Y_1' = 0.53$. At first the interface rises slightly to $y_1' = 0.514$ at the upstream location where $(1 - h') = 1.552$. At the crest, the interface depth has increased to 0.632. At $(1 - h') = 1.031$, the lower-layer Froude number has already reached the value $F_2^2 = 2$. These three positions are marked on the computed sketch and can also be followed on the bold Bernoulli solution curve $Y_1'(q_2')^{-1/3} = 0.9$ in the Froude-number plane (figure 3).

Although the lower layer is dominant and must flow as shown, the upper layer can either flow in the same direction or in the opposite direction to the dominant layer. The Bernoulli equations do not have a direction dependence, and as long as these solutions are stable as discussed by Armi (1986) and Armi & Farmer (1986), they can also represent exchange flows. This is indicated in the sketches by the direction of the non-dominant layer pointing in either direction. These exchange flows with a single control at the crest are in the class of submaximal exchange flows treated by Armi & Farmer (1986).

This two-layer example with a dominant lower layer differs from a single-layer reduced-gravity hydraulic solution with a passive upper layer in a number of ways. First, for the single-layer case, the interface descends to $y_2' = (2/3)(1 - Y_1')$ at the crest, where $(1 - Y_1')$ is the height above the crest in the reservoir. With $(1 - Y_1') = 0.47$, this gives $y_2' = 0.313$ at the crest/narrows. For the two-layer case shown, the descent is somewhat less to $y_2' = 0.368$. The flow rate achieved for the single-layer case, $q_2' = 0.175$, is somewhat less than $q_2' = 0.204$ of the two-layer case for the same interface depth in the upstream reservoir.

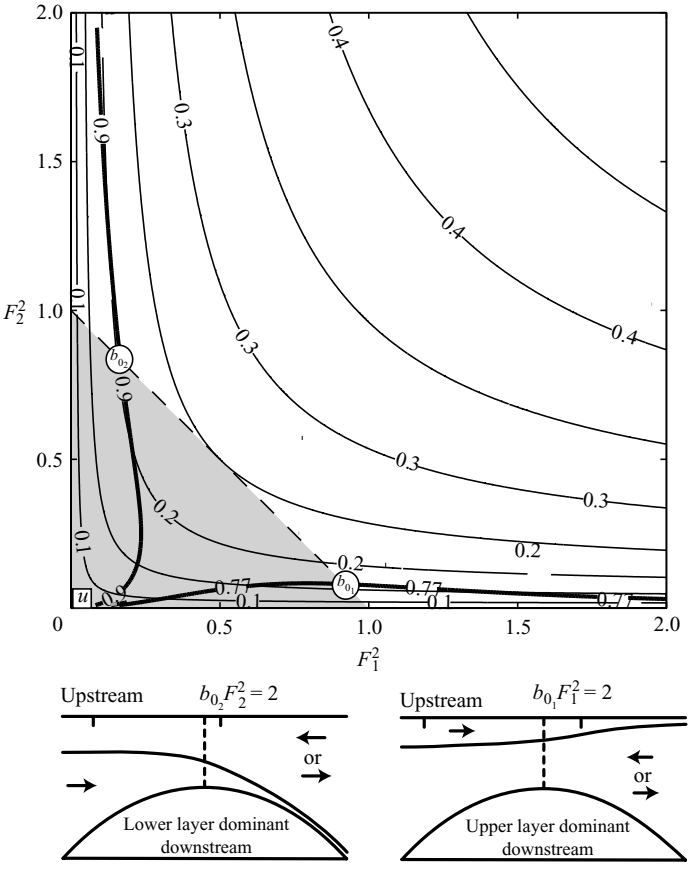

FIGURE 3. Froude-number plane illustrating solution lines $Y_1'(q_2')^{-1/3} = 0.9$ (*lower-layer dominant*), and 0.77 (*upper-layer dominant*). The computed interface shapes of the flows are shown below. $q_r = 1.0$.

	F_1^2	F_2^2	q_2'/b'^2	y_1'	y_2'	u_1'	u_2'	$1-h'$	b'	$Y_1'(q_2')^{-1/3}$	Y_1'
Lower layer dominates											
Upstream u	0.082	0.01	0.055	0.514	1.038	0.207	0.102	1.552	1.933	0.9	0.530
Crest b_{0_2}	0.166	0.835	0.204	0.632	0.368	0.323	0.554	1	1	0.9	0.530
Downstream	0.085	2	0.186	0.765	0.267	0.255	0.730	1.031	1.048	0.9	0.530
Upper layer dominates											
Upstream u	0.1	0.004	0.040	0.404	1.191	0.200	0.068	1.595	2.015	0.77	0.421
Crest b_{0_1}	0.919	0.081	0.164	0.308	0.692	0.533	0.237	1	1	0.77	0.421
Downstream	2	0.031	0.125	0.218	0.875	0.655	0.163	1.093	1.142	0.77	0.421

TABLE 1. Details for the two flows shown in figure 3.

The importance of the upper layer on the dominant lower layer is also evident in the fact that the interface initially rises as the lower layer accelerates towards the crest/narrows (table 1). Although the lower layer dominates the dynamics in the neighbourhood of the crest and downstream, it is not dominant far upstream owing to its large depth. Upstream, both layer Froude numbers are small, yet $F_1^2 \gg F_2^2$.

The response far upstream is given by $(1/y_1)(\partial y_1/\partial x) = F_1^2(1/b)(\mathrm{d}b/\mathrm{d}x)$ (Armi 1986, equation 10*c*) in this limit. Since $(\mathrm{d}b/\mathrm{d}x) < 0$, the interface must initially rise until the lower layer is accelerated and the bottom rises sufficiently to allow it to dominate the dynamics.

This two-layer flow with the lower layer dominant and a co-located crest and narrows differs markedly from the two-layer sill flow streated by Armi (1986). With the constant width assumed in this previous treatment, the upper layer never starts from rest upstream. Inspection of these solutions (Armi 1986, figure 11*a*, *b*) shows that for $F_2^2 = 0$ far upstream, the upper layer always has a finite internal Froude number. For a constant-width crest-controlled flow, the upper layer decelerates as the lower layer is accelerated over the sill crest. Here by including a co-located contraction with the sill, both layers can be at rest in the upstream reservoir.

A flow for which the upper layer dominates is shown on the right-hand side below its solution curve, $Y_1'(q_2')^{-1/3} = 0.77$, in figure 3. The interface position is again drawn to scale and values of the solution parameters at the crest, upstream and downstream can be found in table 1. To distinguish the fact that layer 1, the upper layer, dominates the dynamics we have labelled the crest/narrows as b_{0_1}. In the deep reservoir upstream, the interface depth is $Y_1' = 0.42$; at the crest/narrows it has risen to $y_1' = 0.308$. Downstream, at $(1 - h') = 1.093$, the upper-layer Froude number has already reached the value $F_2^2 = 2$. These three positions are also marked on the computed sketch and can be followed on the bold solution curve $Y_1'(q_2')^{-1/3} = 0.77$ in the Froude-number plane shown in figure 3. Since the upper layer dominates the dynamics in the flow shown, the crest is only felt indirectly by the upper layer through the dynamics of the lower-layer internal Froude number. This can be seen in the influence coefficients derived in Armi (1986, equation 10*a*, *c*). This flow with the upper layer dominant is therefore very similar to the pure contraction flows treated by Armi for which the upper layer was the active layer. As for all these flows with a single control the non-dominant layer can flow in either direction; when it opposes the dominant layer, the flow is in the class of submaximal exchange flows. Maximal exchange flows are treated in the next section.

4. Maximal exchange for a co-located crest/narrows

The maximal exchange for the co-located crest/narrows with $\alpha = 1$ in (2.13) and the computed interface position and topography given by (2.16) is shown in figure 4. This is the pure exchange flow with no barotropic forcing ($q_r = 1$) as discussed by Armi & Farmer (1986) for contractions and Farmer & Armi (1986) for the combination of a sill and contraction. However, the combination cases considered by Farmer & Armi (1986) always had the sill within a constant-width channel and either an exit expansion acting as a control or a contraction before the less dense reservoir (Farmer & Armi 1986, figures 1 and 13). In contrast, the solution shown here is for a co-located contraction/narrows. The interface position is shown to scale and values of the solution parameters are shown at the crest, the virtual control, and on the denser and less dense side where either the upper- or lower-layer Froude number has reached a value of 2.0. The values are also given in table 2.

These maximal exchange flows always have two controls, a topographic control at the crest/narrows and a virtual control on the dense reservoir side of the topographic control. The flow is subcritical between the two controls and supercritical in the direction of the reservoir away from each control. The virtual control is always on the dense fluid side of the crest/narrows.

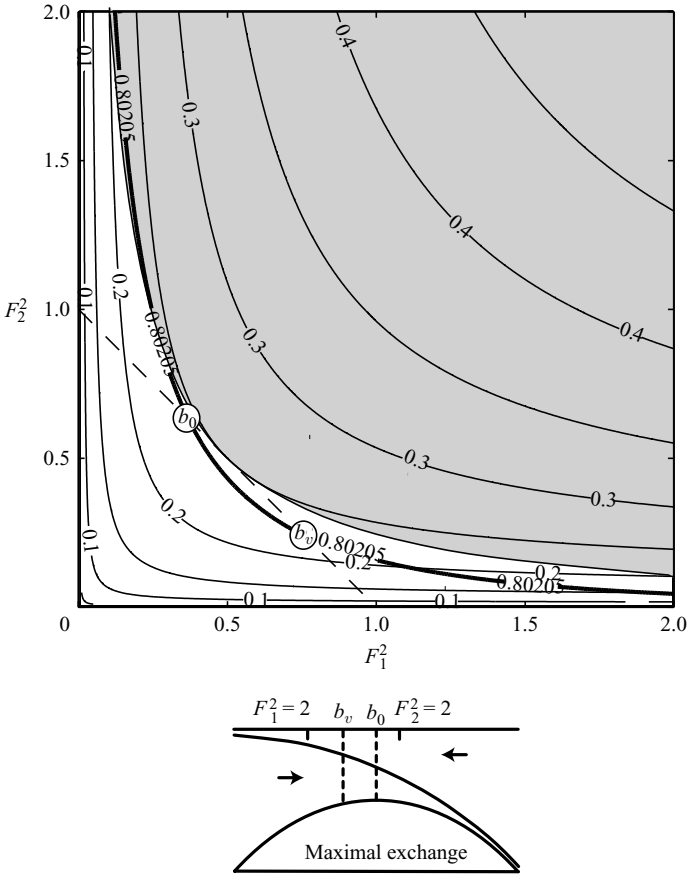

FIGURE 4. Froude-number plane illustrating the maximal exchange flow with the computed interface shape shown below. The stability boundary given by $F_\Delta^2 = 1$ is also shown with the shaded region being unstable. $q_r = -1.0$.

	F_1^2	F_2^2	q_2'/b'^2	y_1'	y_2'	u_1'	u_2'	$1-h'$	b'	$Y_1'(q_2')^{-1/3}$	Y_1'
Denser side	2	0.045	0.146	0.261	0.927	0.724	0.204	1.188	1.295	0.802	0.501
b_v	0.756	0.244	0.226	0.418	0.609	0.562	0.386	1.027	1.040	0.802	0.501
Crest b_0	0.370	0.63	0.244	0.544	0.456	0.449	0.535	1	1	0.802	0.501
Less dense side	0.122	2	0.213	0.751	0.296	0.304	0.771	1.047	1.072	0.802	0.501

TABLE 2. Details for the maximal exchange flow shown in figure 4.

The stability of maximal exchange flows in a pure contraction was studied at the controls by Armi & Farmer (1986) and throughout the contraction by Lawrence (1990). Here, we investigate the stability of the maximal exchange for the co-located crest/narrows. Long (1956) showed that these flows are unstable to even long waves if the stability Froude number

$$F_\Delta^2 = \frac{(u_1 - u_2)^2}{g'(y_1 + y_2)} > 1. \tag{4.1}$$

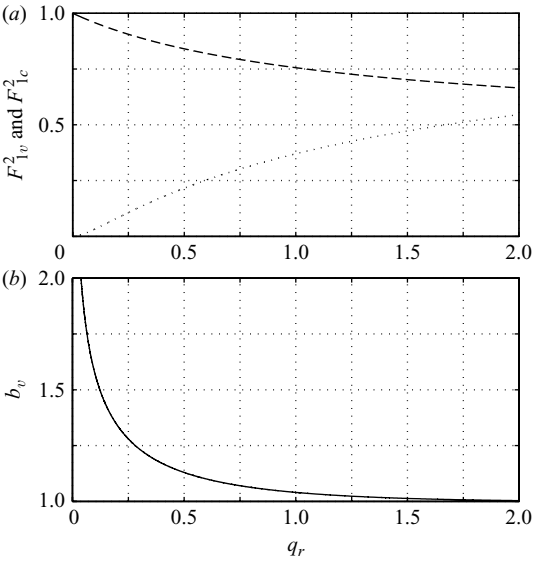

FIGURE 5. (*a*) F_{1v}^2 (dashed line) and F_{1c}^2 (dotted line) are plotted as a function of q_r. (*b*) The width of the channel at the virtual control, b_v, is plotted as a function of q_r.

With (2.2) and (2.3), the stability boundary $F_\Delta^2 = 1$ can be written for exchange flows as

$$\left(q_r^{1/3} F_1^{2/3} - F_2^{2/3}\right)^2 - q_r^{2/3} F_1^{-2/3} - F_2^{-2/3} = 0. \tag{4.2}$$

This boundary is also plotted in figure 4 with the shaded region denoting unstable flows. Unlike the same maximal exchange with $q_r = -1$ in a pure contraction which Lawrence (1990) has shown to be marginally stable everywhere, the maximal exchange in a co-located crest/narrows shown here is stable at both the virtual control and topographic control (the crest/narrows). Only on the less dense reservoir side of the exchange does the flow become unstable as the denser layer accelerates down the slope and the stability boundary is crossed.

To find the maximal exchange for any flow ratio q_r, we note that in figures 2(*a*) to 2(*c*) for $q_r = 1$, 0.5, and 2.0, respectively, there is one saddle point on the surface $Y_1' q_2^{-1/3}(F_1^2, F_2^2)$ which describes the location of the virtual control. It lies on the critical line $F_1^2 + F_2^2 = 1$. Substituting this expression into (2.15) we find:

$$Y_1'(q_2')^{-1/3} = \frac{q_r^{2/3}\left[F_1^{-2/3} + \frac{1}{2}F_1^{4/3}\right] - \frac{1}{2}\left(1 - F_1^2\right)^{2/3}}{\left[q_r^{2/3} F_1^{-2/3} + \left(1 - F_1^2\right)^{-1/3}\right]^{1/2}}. \tag{4.3}$$

There are generally two turning points in this function, a maximum and a minimum. It is at the maximum that the virtual control occurs. We can numerically determine F_{1v}^2 for a range of q_r and also determine the Bernoulli constant $Y_1' q_2^{-1/3}$ at this point. The Bernoulli constant is unchanging along the flow and so we can determine the other point at which its contour crosses the critical line, this is the location of the primary control. In figure 5(*a*), the values of the Froude number at the virtual control, F_{1v}^2, and at the primary control, F_{1c}^2, are plotted as a function of q_r for the maximal flow.

In figure 5(*b*), the width of the channel at the virtual control, b_v, is plotted as a function of q_r. As q_r approaches zero, the flow is concentrated in the bottom layer

and the top layer becomes less dynamic, F_{1c}^2 goes to zero. At the virtual control, only the top layer is dynamically active as F_{1v}^2 approaches unity.

Note that results for the crest/narrows maximal exchange, given in figure 5, lie between the values obtained for a pure contraction (Armi & Farmer 1986, figure 8) and the pure sill with an exit control (Farmer & Armi 1986, figure 7). For example, with no barotropic forcing, $q_r = 1$, at the topographic narrows, $F_{1c}^2 = 0.5$ for the contraction and $F_{1c}^2 = 0.18$ for the sill. For the combined crest/narrows, with the relationship given by (2.13) with $\alpha = 1$, $F_{1c}^2 = 0.37$.

5. Virtually controlled unidirectional flows

As the combined flow rates increase, the two distinct solutions shown in § 3 with either the lower or upper layer dominant are no longer possible. This occurs when the flow rates are high enough that only supercritical conditions can exist at the crest/narrows and the transition from subcritical conditions in the reservoir to supercritical flow occurs upstream of the crest/narrows at a virtual control. This phenomenon was first discovered by Wood (1968). For a contraction with a level bottom and $q_r = 1$, Armi (1986, see figures 6 and 7) found that if $q_2' > 0.25$, a virtually controlled flow always existed with a level interface upstream with no shear between the layers. For these flows to be stable, they must be unidirectional.

An example of the virtually controlled solution for the crest/narrows case is shown in figure 6. For the case shown in figure 6, $q_2' = 0.4126$ at the crest; however, virtual control can appear for flow rates as low as $q_2' = 0.226$. The interface position is shown to scale from the solution found using the Froude-number plane (figure 2*a*) and the topography given by (2.16). Values of solution parameters are also given in table 3 for locations far upstream, the virtual control, the crest/narrows and downstream where either the upper or lower layer will dominate. This will be explained further below.

As the two-layer flow moves from the upstream reservoir, the upper layer accelerates faster than the deeper lower layer. This differs from the pure contraction case for which both layers accelerate at the same rate and their velocities are identical. For the case shown, the virtual control is passed at the non-dimensional width $b_v = 1.352$. At this location, the upper-layer velocity is 46 % larger than the lower-layer velocity.

For the pure contraction, the regularity conditions at the virtual control (Armi 1986, equations 13*a–c*) reduced to

$$\frac{u_1^2}{u_2^2} = 1. \tag{5.1}$$

For a unidirectional flow, this implied no shear, and for exchange flows, equal and opposite velocities at the virtual control. For the combined crest/narrows case, the regularity conditions can be solved including both bottom and width variation to give

$$\frac{u_1^2}{u_2^2} = \frac{\left[1 + \left((\mathrm{d}h'/\mathrm{d}b')\left(F_2^2/y_2'\right)\right)\right]}{\left[1 + \left((\mathrm{d}h'/\mathrm{d}b')\left(F_2^2/y_1'\right)\right)\right]}, \tag{5.2}$$

which reduces to the pure contraction result (5.1) when $(\mathrm{d}h'/\mathrm{d}b') = 0$.

As shown in figure 6, these flows continue to accelerate past the virtual control and in the case shown reach the crest where $q_2' = 0.4126$. The Bernoulli energy constant for the virtually controlled solution is $Y_1'(q_2')^{-1/3} = 0.802$ and is shown in figure 6 starting upstream near the origin and extending past the crest/narrows. However, any small amount of dissipation or any non-hydrostatic effects will cause the actual solution to

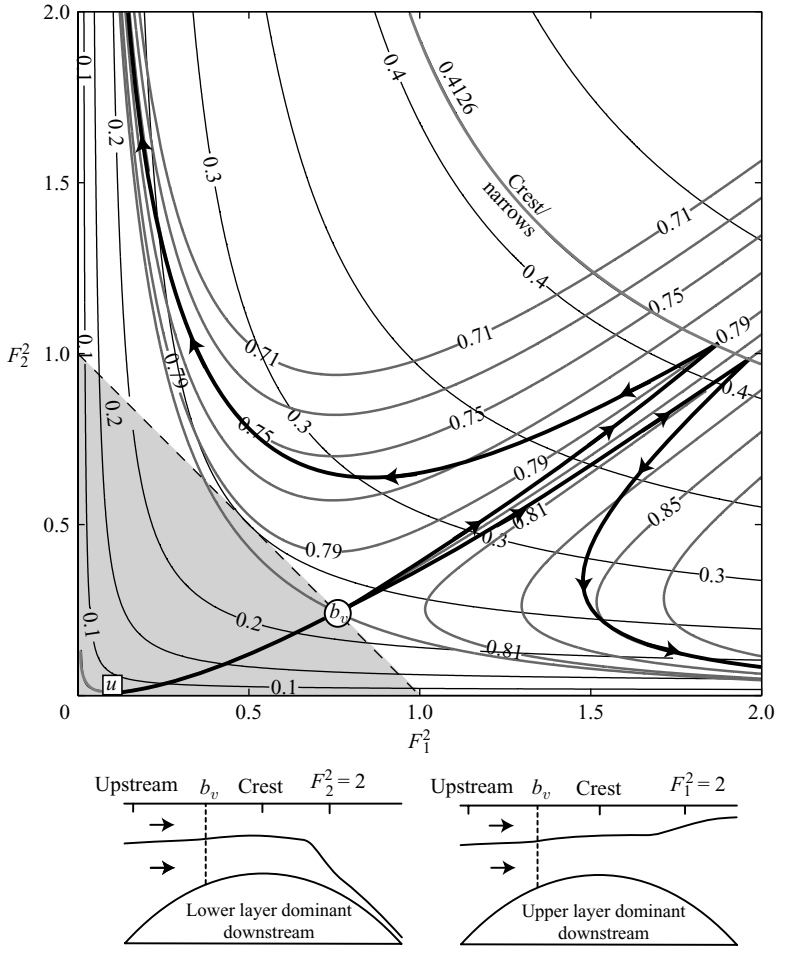

FIGURE 6. Virtually controlled flows with $Y_1'(q_2')^{-1/3} = 0.802$. Upstream and in the neighbourhood of the crest/narrows they are identical, but downstream they each remain supercritical with either the lower or upper layer dominant. $q_r = 1.0$.

	F_1^2	F_2^2	q_2'/b'^2	y_1'	y_2'	u_1'	u_2'	$1-h'$	b'	$Y_1'(q_2')^{-1/3}$	Y_1'
Upstream u	0.135	0.01	0.059	0.565	1.346	0.276	0.116	1.911	2.642	0.802	0.597
Virtually controlled b_v	0.756	0.244	0.226	0.497	0.725	0.615	0.422	1.223	1.352	0.802	0.597
Crest	1.923	1	0.413	0.446	0.554	0.926	0.746	1	1	0.802	0.597
Upper layer dominates	2	0.084	0.185	0.337	0.970	0.821	0.285	1.307	1.493	0.850	0.597
Lower layer dominates	0.151	2	0.229	0.855	0.362	0.359	0.851	1.217	1.342	0.750	0.597

TABLE 3. Details for the virtually controlled flows shown in figure 6.

move away from this ideal solution as the flow accelerates past the virtual control to the crest and then starts to decelerate downstream of the crest. There are two possible paths shown in the Froude-number plane with the associated interface shapes in figure 6. Neither of these virtually controlled flows decelerate through the apparent

symmetrical location on the downstream side of the virtual control passed through on the upstream side. As shown for a pure contraction with laboratory experiments and the equivalent Froude-number plane for a pure contraction (Armi 1986) the flows do not return to subcritical values reached at the corresponding width upstream. The flows diverge along either of the solutions shown with an acceleration of either the lower or upper layer downstream.

For the flow shown on the right, the upper layer dominates the dynamics as the flow remains supercritical downstream. For the flow shown on the left, the lower layer dominates the dynamics as the flow remains supercritical downstream. Which of these two possible paths is taken depends on matching conditions downstream. For the case in which the lower layer dominates, the interface position downstream will be deeper than in the reservoir upstream and matching can be achieved with an internal hydraulic jump in which the lower layer is dominant. For the case in which the upper layer dominates, the interface position downstream will be shallower than in the upstream reservoir. The matching is then through an inverted internal hydraulic jump in which the upper layer is dominant.

6. Conclusion

The Froude-number plane approach to two-layer hydraulics has the significant benefit that all possible solutions can be seen at once. The flows are parameterized with the internal Froude numbers for each layer and conditions for critical flow are simply a straight line separating subcritical and supercritical flows. Flow paths in the plane then follow lines along which the Bernoulli function is constant and the non-dimensional flow rate per unit width or depth varies through the topography. This approach was previously limited by the need to use separate planes for width variation and bottom depth variation. Here we have removed this limitation by allowing the topography to vary in such a way that the non-dimensional total depth and the non-dimensional width are everywhere given by a very general algebraic relationship (2.13). The crest/narrows are co-located, but the actual shape can be quite general.

The main results are summarized in figures 3, 4 and 6 which show typical paths in the new Froude-number plane for a co-located crest/narrows. There are five possible asymmetric paths. Two paths with a single control at the crest/narrows were discussed first in § 3. The flow with the upper layer as the dominant layer is similar to the previously treated pure contraction flow. The case with a dominant lower layer is new since the flow can now start from rest in the upstream reservoir. The earlier treatment for bottom variation in a constant-width channel was limited because the upper layer never came to rest in the upstream reservoir.

The maximal exchange for the combined crest/narrows appears on the lighter reservoir side to be similar to the previously treated sill case whereas on the dense water side it has the character of the pure contraction with a virtual control acting as the second control. The nature of the virtual control is now quite different since the speeds in the each of the opposing layers are no longer equal.

Virtually controlled flows for the two layers flowing in the same direction are similar to those found for the pure contraction except for the nature of the virtual control. No longer does the flow behave as an unsheared flow with no internal dynamics. The regularity conditions at the virtual control are more complicated since both width and bottom variations are now acting on the flow. Downstream where the flow remains

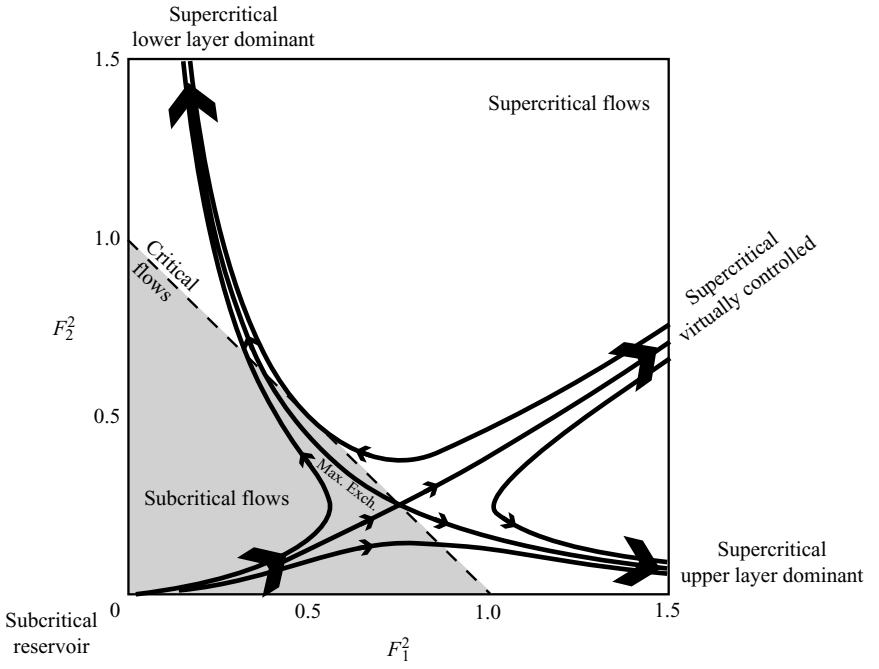

FIGURE 7. Flow paths through and in the neighbourhood of the virtual control saddle-point.

supercritical it either acts like the contraction case when the upper layer is dominant or a sill flow when the lower layer is dominant.

These five possible flow paths can be seen in the neighbourhood of the virtual control in figure 7. The virtual control is the only location in the Froude-number plane where two lines with the same value of the Bernoulli constant cross. One line represents the maximal exchange flow while the straighter line represents virtually controlled flows that can start from rest in an upstream reservoir. On figure 7, the direction towards supercritical flow is indicated near the virtual control with arrows.

Flows in the neighbourhood of the virtual control with a somewhat lower flow rate starting subcritically in an upstream reservoir are controlled by the crest/narrows on either side of the virtual control in the Froude-number plane, as the upper layer becomes supercritical or the lower layer becomes supercritical downstream. As the flow rates increase, only the virtually controlled path is possible from the upstream reservoir. The arrows show the controlled flows diverging about the location of the virtual control with only the unidirectional virtually controlled flow passing from subcritical conditions in an upstream reservoir to supercritical flow, with both layers dynamically active downstream along the nearly straight line.

The crossing maximal exchange flow is a somewhat special flow since the subcritical portion of this flow is small, not a stagnant reservoir, and links the topographic control at the crest/narrows with the virtual control. However, the arrows are always away from the subcritical region since the flow is supercritical on either side of this portion of the flow.

At the crest/narrows control, the constant continuity (q_2'/b'^2) and Bernoulli ($Y_1'(q_2')^{-1/3}$) curves are tangent, as can be seen by inspection of figure 2 and the summary figures 3, 4 and 6. In contrast, the virtual control is at a saddle-point of the Bernoulli function located on the critical flow line. The continuity function is

not tangent to the Bernoulli function at the virtual control location, and the virtual control regularity condition must be satisfied for the flows to pass through the virtual control either in a maximal exchange flow or as a unidirectional flow.

From the arrows on the diagram, it can also be seen that a virtually controlled flow that was accelerated to supercritical flow through an upstream virtual control before the crest/narrows must deviate in the neighbourhood of the location predicted from symmetry alone for a virtual control downstream of the crest/narrows. There are always paths with almost the same value of the Bernoulli constant near the location of this point that can be reached from the supercritical portion of the Froude-number plane as the flow decelerates and allow the flow to remain supercritical and for one of the layers to accelerate downstream. These are also indicated by arrows in the neighbourhood of the virtual control reachable only from the supercritical side.

L. A. thanks The University of California and Lucky Larry's Auto Repair for sustained financial support of his interest in two-layer flows. U. R. thanks Dr D. A. Smeed and Professor P. D. Killworth for making her PhD possible which inspired this work.

REFERENCES

Armi, L. 1986 The hydraulics of two flowing layers with different densities. *J. Fluid Mech.* **163**, 27–58.

Armi, L. & Farmer, D. M. 1986 Maximal two-layer exchange through a contraction with barotropic net flow. *J. Fluid Mech.* **164**, 27–51.

Dalziel, S. B. 1991 Two-layer hydraulics: a functional approach. *J. Fluid Mech.* **223**, 135–163.

Dalziel, S. B. 1992 Maximal exchange in channels with nonrectangular cross section. *J. Phys. Oceanogr.* **22**, 1188–1206.

Engqvist, A. & Hogg, A. McC. 2004 Unidirectional stratified flow through a non-rectangular channel. *J. Fluid Mech.* **509**, 83–92.

Farmer, D. M. & Armi, L. 1986 Maximal two-layer exchange over a sill and through the combination of a sill and contraction with barotropic flow. *J. Fluid Mech.* **164**, 53–76.

Gill, A. E. 1977 The hydraulics of rotating-channel flow. *J. Fluid Mech.* **80**, 641–671.

Lawrence, G. A. 1990 On the hydraulics of Boussinesq and non-Boussinesq two-layer flows. *J. Fluid Mech.* **215**, 457–480.

Lawrence, G. A. 1993 The hydraulics of steady two-layer flow over a fixed obstacle. *J. Fluid Mech.* **254**, 605–633.

Long, R. R. 1956 Long waves in a two-fluid system. *J. Met.* **13**, 70–74.

Riemenschneider, U., Smeed, D. A. & Killworth, P. D. 2005 Theory of two-layer hydraulic exchange flows with rotation. *J. Fluid Mech.* **545**, 373–395.

Wood, I. R. 1968 Selective withdrawal from a stably stratified fluid. *J. Fluid Mech.* **32**, 209–223.